Measurement of the Spin-Orbit Perturbation in the P-State Continuum of Heavy Alkali-Metal Atoms: K, Rb, and Cs†

J. Baum, M. S. Lubell, and W. Raith
Yale University, New Haven, Connecticut 06520
(Received 12 October 1971)

The spin-orbit interaction for the P-state continuum of heavy alkali metals was investigated in a photoionization experiment using spin-polarized alkali atoms and circularly polarized light. From the asymmetry in ion-counting rates corresponding to the two photon helicities, Fano's spin-orbit perturbation parameter x was determined over a range of several hundred angstroms for K, Rb, and Cs. The spin-orbit perturbation was found to increase from K to Rb to Cs as expected, and the nonlinear behavior of x as a function of the photon energy E was demonstrated for K. Knowledge of $x(E)$ was used to establish accurate values for the position of the Cooper minimum and to estimate the magnitude of the cross section at the minimum. In addition, the $x(E)$ data for Cs were used to gain information about the spin polarization of photoelectrons in a Fano-type polarized electron source. Finally, extrapolation of $x(E)$ for cesium into the discrete spectrum indicated the existence of a pole in the function $\rho(E)$ which corresponds to the doublet line-strength ratio $\rho(E_{nP}) = S(nP_{3/2})/S(nP_{1/2})$ at the discrete energies E_{nP}. According to our extrapolation, the pole lies in the region of $n = 10$ to 15, in agreement with the early spectroscopic work of Sambursky (1928) and Beutell (1939), whose measurements were discounted by later investigators.

I. INTRODUCTION

For an electron in the electric field of an atom or ion, the interaction between its spin and orbital angular momentum is weak compared with the Coulomb interaction, usually causing only a minor perturbation. Nevertheless, the spin-orbit interaction can lead to well-known conspicuous effects[1] such as the polarization effects in Mott scattering of electrons from heavy atoms, as well as the fine-structure energy splitting and the associated anomalous doublet line-strength ratios of the discrete P states of the heavy alkali-metal atoms. This paper deals with the pronounced spin-orbit effect (Fano effect) in alkali photoionization.

As a vehicle for describing the spin-orbit perturbation, Fano[2] introduced a perturbation parameter x which is a function of the photon energy E and is defined by

$$x = 3R^0(E)/\Delta R(E) \tag{1.1}$$

with

$$\begin{aligned} 3R^0 &= 2R_3 + R_1 , \\ \Delta R &= R_3 - R_1 , \end{aligned} \tag{1.2}$$

where R^0 is the unperturbed radial matrix element for the dipole transition from the $n_0{}^2S_{1/2}$ ground state, and R_3 and R_1 are the perturbed radial matrix elements for the final P-state angular momenta $J' = \frac{3}{2}$ and $\frac{1}{2}$, respectively. Quantitative knowledge of the strength of the spin-orbit perturbation permits separation of this effect from other perturbations such as core polarization and configuration interaction, thus facilitating a more accurate interpretation of observed spectroscopic anomalies.[3,4] In addition, for the construction of proper alkali-metal-atom wave functions, data on the spin-orbit perturbation provide a useful supplement to data on energy eigenvalues, since the former are most sensitive to the wave functions at small radii while the latter depend more on the wave functions at large radii.

As will be shown in Sec. II, the parameter $x(E)$ determines all polarization effects in photoionization and also enters into the formula for the energy dependence of the photoionization cross section $\sigma(E)$. For $E < E_{\text{th}}$, where E_{th} is the photon energy of the ionization threshold, $x(E)$ is physically meaningful only at the photon energies which correspond to resonance transitions $n_0S \rightarrow nP$. However, $x(E)$ can be plotted as a continuous function which goes smoothly through threshold, analogous to the behavior of the oscillator-strength density[5] and the quantum defect.[6,7] In the discrete spectrum, $x(E_{nP})$ determines the doublet line-strength ratio,

$$\begin{aligned} \rho(nP) &= S(nP_{3/2})/S(nP_{1/2}) \\ &= 2(x+1)^2/(x-2)^2, \end{aligned} \tag{1.3}$$

where $S(nP_{3/2})$ and $S(nP_{1/2})$ are the line strengths of the doublet lines D_2 and D_1, respectively. Estimates for $x(E)$ can be obtained in the discrete spectrum from measurement of $\rho(nP)$ of low-lying P states and in the continuum from data on $\sigma(E)$. As Fano pointed out, accurate values of $x(E)$ can be obtained from polarization experiments on photoionization in the vicinity of the cross-section minimum.[2]

We performed an experiment involving photoionization of spin-polarized alkali-metal atoms by

monochromatic circularly polarized light. The experiment yielded values of $x(E)$ for potassium, rubidium, and cesium at photon energies in the near ultraviolet. This paper is the first detailed account of the experimental work. Brief reports of this research have already been communicated.[8-14]

II. THEORETICAL BACKGROUND

We restrict our considerations to electric-dipole transitions from the $n_0{}^2S_{1/2}$ ground state of the alkali-metal atom ($n_0 = 4$, 5, 6 for K, Rb, Cs, respectively) to discrete and continuum P states. As an energy parameter we use the photon energy $E = E_{th} + \epsilon$, where ϵ is the binding energy of the final discrete P state for $E < E_{th}$ and the photoelectron energy for $E > E_{th}$. We assume an average over all directions of photoelectron emission, so that only the radial part of matrix elements and wave functions need be considered. The radial matrix elements R_3 and R_1, as well as the perturbation parameter x, are real functions of the photon energy.

A. Photoionization Cross Section

For alkali-metal atoms, the P-state wave functions have nodes in the region of maximum overlap with the ground-state wave functions. As a consequence, a great deal of cancellation occurs in the dipole-transition matrix element. At some photon energy E_0 the matrix element passes through zero. For lithium, E_0 lies below E_{th}[15]; for the other alkali metals, E_0 lies above E_{th}. When the matrix element passes through zero, the photoionization cross section $\sigma(E)$ goes through a Cooper minimum,[16] which is exhibited by all alkali-metal atoms heavier than lithium.

Measurements of $\sigma(E)$ show that the minimum cross section is different from zero for K, Rb, and Cs. In 1951 Seaton[17] pointed out that any central-field calculation "almost certainly" would yield a zero-minimum cross section, and therefore he suggested spin-orbit perturbation as the only likely explanation of $\sigma_{min} > 0$. Extending Fermi's spin-orbit perturbation theory[18] to the continuum P states, Seaton obtained estimates of σ_{min} which gave an order-of-magnitude agreement with the experimental data for Rb and Cs but not for K. This discrepancy will be discussed in Sec. V B.

With the inclusion of spin-orbit perturbation, the radial matrix elements R_3 and R_1 differ from each other; in particular, they go through zero at different energies. The expression for the photoionization cross section, written as

$$\sigma(E) = C\,E\{2[R_3(E)]^2 + [R_1(E)]^2\}, \qquad (2.1)$$

with C as a constant, shows that zero points of $R_3(E)$ and $R_1(E)$ at different energies lead to a nonzero minimum of $\sigma(E)$. Using the notation introduced in Eqs. (1.1) and (1.2), we can write the cross section as

$$\sigma(E) = \tfrac{1}{3} C\,E[\Delta R(E)]^2\{2 + [x(E)]^2\}. \qquad (2.2)$$

As a first approximation, valid only for a small energy interval in the vicinity of the Cooper minimum, we can assume that $R^0(E)$ is a linear function while $\Delta R(E)$ is constant. On this basis Fano[2] deduced an estimate of $x(E)$ for cesium by fitting a parabola to the cross-section data of Marr and Creek[19] according to

$$\sigma(E) \approx \sigma_{min}\{1 + \tfrac{1}{2}[x(E)]^2\}. \qquad (2.3)$$

Fano emphasized that the value of $x(E)$ obtained in this way should be used only "most tentatively" for indicating the magnitude of polarization effects. Since this estimate has been regarded as a theoretical prediction,[20,21] we would like to point out that the results contained in the present paper, although numerically different from Fano's estimate, fully confirm his theory.

B. Polarization Effects in Photoionization

In alkali-metal atoms the electronic spin S and the nuclear spin I are coupled, forming the total angular momentum F. The influence of the nuclear spin on the photoionization process, however, can be neglected.[2] Thus only the electronic polarization of the atom and the polarizations of the electron and photon need be considered. (The outgoing ion has only nuclear polarization.) We define the electronic polarization of the atom as

$$P_{at} = \langle \sigma_z \rangle = \langle 2m_S \rangle, \qquad (2.4)$$

where σ_z is the Pauli matrix operator for the spin component along the axis of quantization determined by the external magnetic field $\vec{B}$, and $\langle 2m_S \rangle$ is twice the expectation value of the electronic-spin magnetic quantum number. The spin polarization of the outgoing photoelectron is defined as

$$P_{el} = \langle 2m'_S \rangle, \qquad (2.5)$$

with reference to the same axis of quantization as that for the atom. Finally, for photons incident parallel to the magnetic field $\vec{B}$, the photon spin polarization is given by

$$P_{ph} = \langle m_{ph} \rangle. \qquad (2.6)$$

The degree of circular light polarization is equivalent to P_{ph}.

The transition matrix elements in the $|L, S, m_L, m_S\rangle$ representation can be written in the general form shown in Fig. 1. The final state, $|E; L' = 1, S' = \frac{1}{2}, m'_L, m'_S\rangle$, is a continuum P state with $m'_L = +1$, 0, or -1, with the proper value of m'_L determined by conservation of angular momentum ($m'_L = m_{ph} + m_S - m'_S$). Thus the transitions for which the matrix element is listed as zero are forbidden. The spin-orbit interaction is taken into

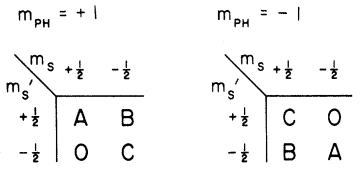

FIG. 1. Matrices for dipole transitions with spin-orbit interaction. The magnetic quantum numbers m_S', m_S, and m_{ph} refer to spin states of atomic electron, photoelectron, and photon, respectively.

account by $A \neq C$ and $B \neq 0$.

The perturbation parameter x was introduced in Eqs. (1.1) and (1.2) in terms of R_1 and R_3, the radial matrix elements for the transitions to final angular-momentum states which are eigenstates in the $|L, S, J, m_J\rangle$ representation. The matrices of Fig. 1, however, refer to $|L, S, m_L, m_S\rangle$ eigenstates. With the use of the appropriate Clebsch-Gordan coefficients, the elements A, B, and C can be related to R_3 and R_1,[2] and thereby to x. With all common numerical factors omitted the following results are obtained:

$$A = 3R_3 = \Delta R(x+1) ,$$
$$B = \sqrt{2}\,(R_3 - R_1) = \Delta R\,\sqrt{2} , \qquad (2.7)$$
$$C = R_3 + 2R_1 = \Delta R(x-1) .$$

The photoionization cross section is proportional to E times the sum of the square of matrix elements. From Fig. 1 and Eqs. (2.4)–(2.7) it can then be shown that the cross section for photoionization of *polarized* atoms by *polarized* photons is given by

$$\sigma(E, P_{ph}, P_{at}) = f(E)\,[(x^2+2) + (2x-1)\,P_{ph}\,P_{at}] , \qquad (2.8)$$

where $f(E) = (\text{const})\,E[\Delta R(E)]^2$ is a function of the photon energy, independent of P_{ph} and P_{at}. The polarization of the outgoing electron is given by

$$P_{el} = \frac{(2x+1)\,P_{ph} + x^2 P_{at}}{(x^2+2) + (2x-1)\,P_{ph}\,P_{at}} . \qquad (2.9)$$

With unpolarized atoms and unpolarized photons, Eq. (2.8) reduces to Eq. (2.2), and P_{el} given by Eq. (2.9) vanishes. With either one of the incoming particles polarized (photons or atoms) the cross section is still given by Eq. (2.2). However, the electron polarization is nonzero. The two polarization parameters which can thus be determined by a polarization measurement of the outgoing photoelectrons are

$$P \equiv [P_{el}/P_{ph}]_{P_{at}=0} = (2x+1)/(x^2+2) \qquad (2.10)$$

and

$$R \equiv [P_{el}/P_{at}]_{P_{ph}=0} = x^2/(x^2+2) . \qquad (2.11)$$

With both incoming particles polarized the cross section is now given by Eq. (2.8). From counting rates C^+ and C^- of photoionization events corresponding to positive and negative signs of the product $P_{ph}P_{at}$, respectively, a third polarization parameter Q can be determined. With the asymmetry δ defined by

$$\delta \equiv (C^+ - C^-)/(C^+ + C^-) \qquad (2.12)$$

and the corresponding cross sections obtained from Eq. (2.8), it follows that Q is given by

$$Q \equiv \delta/|P_{ph}P_{at}| = (2x-1)/(x^2+2) . \qquad (2.13)$$

The functions $P(x)$, $Q(x)$, and $R(x)$ are plotted in Fig. 2.

The spin-orbit perturbation pushes out the $P_{3/2}$ radial wave functions and pulls in the $P_{1/2}$ functions. It therefore follows that $R_3(E)$ goes through zero at a higher photon energy than $R_1(E)$. Equations (1.1) and (1.2) then show that the slope dx/dE is negative. In order to achieve visual similarity among figures, the x axis in Fig. 2 was chosen to point from right to left.

As Fano pointed out in a later paper,[22] a small correction is necessary to take into account the phase difference in the normalization of the wave functions of the $P_{3/2}$ and $P_{1/2}$ photoelectrons. Thus Eq. (2.7) should be modified by multiplying R_3 and R_1 with phase factors $e^{i\varphi_3}$ and $e^{i\varphi_1}$, respectively, and by introducing a complex perturbation parameter $z = x + iy$. Because a Q measurement does not distinguish between spin states in the outgoing

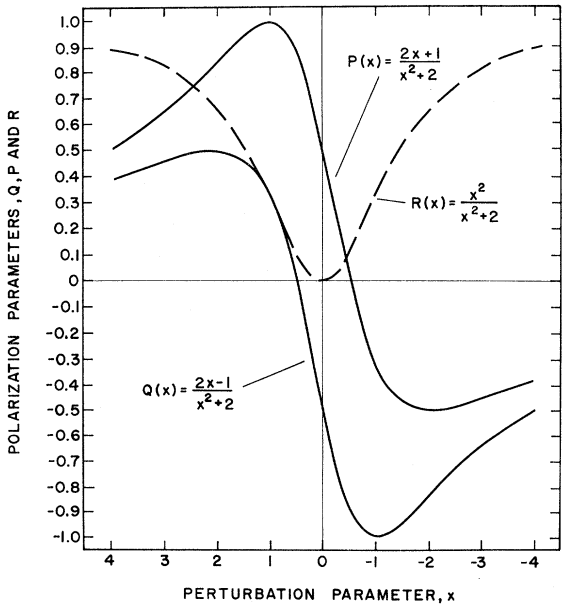

FIG. 2. Polarization parameters P, Q, and R as functions of the perturbation parameter x. Note that x increases from right to left.

channel, Eq. (2.13) remains unchanged. However, Eqs. (2.10) and (2.11) for $P(x)$ and $R(x)$ can only be retained as approximations. The phase difference $\Delta\varphi = \varphi_3 - \varphi_1$ is related to quantum defect τ by

$$\Delta\varphi = \pi\Delta\tau , \tag{2.14}$$

where $\Delta\tau$ is extrapolated into the continuum from the values $\Delta\tau = \tau(nP_{1/2}) - \tau(nP_{3/2})$ in the discrete spectrum. The values of the quantum-defect lag $\Delta\tau$ are 0.0029, 0.013, and 0.032 for K, Rb, and Cs, respectively.[1] Since the corrections are of the order of $\sin^2\Delta\varphi$, they are far too small to be detected with present techniques available for measurements of P or R.

III. EXPERIMENTAL ARRANGEMENT AND PROCEDURE

A. Choice of Method

With present technology, a measurement of Q can be executed with significantly higher accuracy than a measurement of P or R for the following reasons.

(a) The relative ease of producing and detecting polarized particles is displayed by the figure of merit, $M = \mathcal{P}^2\eta$, where $\mathcal{P}$ is the degree of polarization produced (or the analyzing power of a polarization detector) and η is the intensity attenuation accompanying the production (or detection) of the polarization. The respective figures of merit are approximately 1.6×10^{-1}, 4.5×10^{-3}, and 6.3×10^{-5} for photons, atoms, and electrons.[23] For any given statistical accuracy the time t required for a measurement of P, Q, or R is proportional to product of the two relevant figures of merit. Thus we find $t_P \propto M_{\rm ph}M_{\rm el} \sim 10^{-5}$, $t_Q \propto M_{\rm ph}M_{\rm at} \sim 8\times10^{-4}$, and $t_R \propto M_{\rm at}M_{\rm el} \sim 3\times10^{-7}$.

(b) Photoelectrons from walls provide a large background which must be distinguished from the signal resulting from the atomic-beam photoelectrons. In the Q measurement (which does not require polarization analysis of the photoelectrons) ions can be detected rather than electrons.

(c) The theoretical relations given in Secs. I and II contain only the radial parts of the matrix elements, since they represent averages over all directions of photoelectron emission. There are, however, angular dependences in the polarization effects[22,24] and deviations can be expected if the experimental averaging is incomplete. If electrons are detected, careful attention must be paid to this problem, particularly at the higher photon energies for which the initial electron energies are electron-optically significant. With ion detection in a Q measurement, the directional averaging is not a problem, since the recoil energy of the ion is negligible.

For these three compelling reasons we chose to measure Q rather than P or R. The main advantage for pursuing a measurement of P or R is that the required apparatus can be regarded as a source of polarized electrons at the photon wavelengths for which P or R are close to unity. The requirements for optimum performance of such a source, however, are so different from the requirements for an accurate determination of x that these two goals have been pursued separately in this laboratory. In this paper, we report only the work on the measurement of the strength of the spin-orbit perturbation. Parallel to this work, a polarized electron source, based on photoionization of unpolarized cesium atoms by circularly polarized light and designed for yielding a high current of highly polarized electrons with a small energy spread, has been built and tested[25] and is now being employed in an e-H low-energy scattering experiment. A detailed report on this polarized electron source will be published separately.

B. Apparatus

The apparatus, shown schematically in Fig. 3, was a crossed-beam system. An atomic beam produced by effusion from an oven and state selected by passage through a permanent six-pole magnet was intersected by a monochromatic, circularly polarized light beam. In the interaction region a weak magnetic field of 2 G (produced by Helmholtz coils not shown in Fig. 3) was applied parallel to the incident light beam. The atomic-beam intensity was monitored by means of a hot-wire detector; the light intensity was monitored by a photocell. The alkali-metal ions produced in the interaction region were accelerated onto the cathode of an electron multiplier and counted. As seen from Eq. (2.8), measurement of the polarization parameter Q as a function of the photon energy E requires polarization of atom and photon beam and measurement of the ion-counting-rate asymmetry $\delta(E)$. Since the six-pole magnet produced only positive atomic polarization the photon polarization was reversed for measuring the counting rates C^+ and C^-. Details of the system are discussed below.

Atomic-beam system. In order to lower the molecular content in the atomic beam the alkali-metal oven was designed as a two-chamber oven with reduced vapor pressure and increased temperature in the second chamber from which the beam emerged through an orifice 0.1 cm in diam. After preliminary measurements indicated that the two-chamber design did not reduce the molecular content sufficiently, a central beam stop 0.16 cm in diam was inserted 1.8 cm upstream from the entrance to the six-pole magnet and 5.6 cm downstream from the oven orifice. This stop blocked the line of sight between the oven orifice and magnet exit. Since alkali-metal molecules

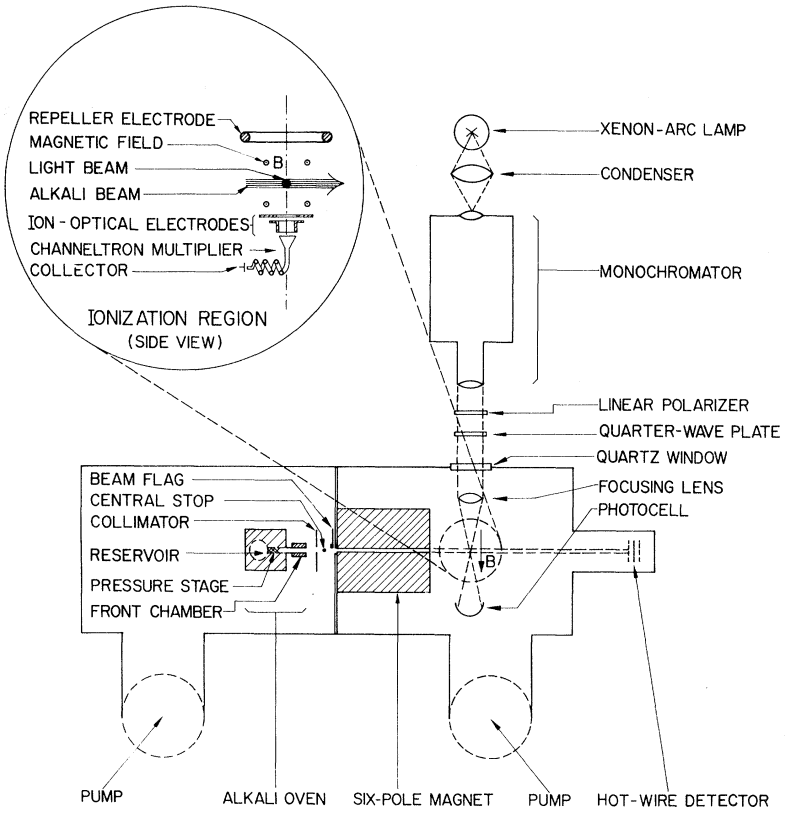

FIG. 3. Schematic diagram of the experimental apparatus (drawn in top view, except for enlarged part).

are not affected by inhomogeneous magnetic fields and therefore travel on straight trajectories, they were eliminated from the beam completely. The six-pole magnet was 17.5 cm long and had a gap diameter of 0.32 cm. The magnetic field at the pole tips was approximately 8500 G. A detailed discussion of the molecular content in alkali-metal beams and the focusing properties of six-pole magnets was presented in a previous publication.[26] Highly purified alkali metal in 2-g glass ampoules was used for loading the oven. The ampoules were cracked inside the oven in an argon atmosphere.

Optical system. Light from a xenon high-pressure arc lamp (Hanovia No. 959-C) was passed through a grating monochromator (Bausch and Lomb Nos. 33-86-25 and 33-86-01) whose slits were set for a spectral resolution of $\Delta\lambda = 16$ Å.[27] The monochromator was calibrated with a mercury spectral lamp. As a linear polarizer we employed a dichroitic film (Polacoat PL40) deposited onto a fused-quartz plate. The quarter-wave plate (B. Halle Nachf., Berlin) consisted of two crystal-quartz plates, sandwiched together with their fast axes 90° apart and ground to a thickness difference such that the resulting optical-path difference for the two polarization states was $\frac{1}{4}\lambda$ at $\lambda = 2800$ Å. This provided a high degree of circular polarization over a wide spectral range (cf. Fig. 5). Both the linear polarizer and quarter-wave plate were mounted in rotatable holders. The light was focused onto the atomic beam by Suprasil quartz lenses. Several well-blackened apertures (not shown in Fig. 3) were built into the vacuum chamber to reduce stray light. The light intensity was continuously monitored by means of a photocell with S-5 spectral sensitivity.

Ion-detection system. The alkali-metal ions produced by photoionization were accelerated vertically down (cf. enlargement of Fig. 3) onto the mouth of a Channeltron multiplier (Bendix No. 4028). The repeller electrode above the ionization region was at potential of +4 kV, and the mouth of the Channeltron was at −3.3 kV. The electrodes in front of the multiplier were at variable negative potentials optimized for ion transfer.

C. Photon Polarization

The determination of P_{ph} is straightforward in principle, but was somewhat complicated in practice because the optical elements were not ideal. The light emerging from the monochromator was not unpolarized; the linear polarizer was imperfect; and the quarter-wave plate was a true $\frac{1}{4}\lambda$ plate only at $\lambda = 2800$ Å. Since these instrumental effects were all wavelength dependent, the measurement of P_{ph} had to be carried out over the entire

wavelength range used (3200–2200 Å).

The light leaving the optical system contained an unpolarized component and an elliptically polarized component. Therefore the light must be characterized by a total polarization $P_{tot} < 1$. By P_{ph}, however, is meant the degree of circular polarization. From considerations of polarization vectors in Poincaré space[28] it can be shown that P_{ph} and P_{tot} are related by

$$P_{ph} = [P_{tot}^2 - P_{lin}^2]^{1/2} , \quad (3.1)$$

where P_{lin} is the degree of linear polarization. The determination of P_{ph} was accomplished by separate measurements of P_{lin} and P_{tot}.

For both of these measurements a linear analyzer was introduced. The intensity modulation $\mathfrak{M}$ produced by the rotation of the analyzer was measured for the following two cases: (i) settings of the quarter-wave plate which produced minimum modulation and were used in the photoionization experiment, and (ii) settings of the quarter-wave plate which produced maximum modulation at each wavelength. The intensity modulation $\mathfrak{M}$ is proportional to the degree of linear polarization p of the light incident upon the analyzer. This leads to $p = P_{lin}$ for case (i) and $p = P_{tot}$ for case (ii).

If I_{max} and I_{min} denote, respectively, the maximum and minimum transmitted intensity, $\mathfrak{M}$ is given by

$$\mathfrak{M} = (I_{max} - I_{min})/(I_{max} + I_{min}) . \quad (3.2)$$

If the analyzer had been ideal, p would have been equal to $\mathfrak{M}$. However, the analyzer had finite transmittances for both polarization states. For linearly polarized incident light the analyzer can be characterized by two transmittances T and t corresponding, respectively, to positions for maximum and minimum transmission. Both transmittances were wavelength dependent. Under these nonideal circumstances p is given by

$$p = [(1+\tau)/(1-\tau)]\mathfrak{M} , \quad (3.3)$$

where $\tau = t/T > 0$. In a separate measurment $\tau(\lambda)$ was determined using the analyzer together with a linear polarizer and was found to vary between 0.05 and 0.01 over the wavelength range $\lambda = 3150$ to 2200 Å. A check was made to ensure that the polarizer and analyzer had the same optical properties.

The light measurements were further complicated by the fact that the monochromator transmitted some stray light. The presence of the stray light was detected through the use of a filter whose transmission curve is shown in Fig. 4. With the monochromator dial set at $\lambda < 2600$ Å and the filter inserted, the S-5 photocell continued to detect light. From cesium ion-counting-rate measurements it was established that the stray light was of wavelengths longer than 3200 Å. As seen from Fig. 4, the ratio of the counting rates with filter "in" and filter "out" displayed the same wavelength dependence as the filter transmission curve. In other words, the stray light which remained when the filter was inserted corresponded to photons of energy less than $E_{th}(\mathrm{Cs}) < E_{th}(\mathrm{Rb}) < E_{th}(\mathrm{K})$. Since the polarization of the stray light differed from the polarization of the light proper, the stray light had to be subtracted from the photocell signal during the measurement of the modulation $\mathfrak{M}$ given by Eq. (3.2). This subtraction was achieved by moving the filter in and out of the light beam while the analyzer was rotated. Only that part of the light signal which was doubly modulated was used for the determination of $\mathfrak{M}$.

Checks were made to ensure that the quartz window and the lens mounted inside the vacuum chamber (see Fig. 3) did not alter the light polarization. In our data-taking procedure four different combinations of polarizer settings were employed for obtaining circularly polarized light. The light polarization was measured for each of these settings, and the four polarizations were averaged. The result $P_{ph}(E)$ is presented in Fig. 5. The proper sign of $P_{ph} = \langle m_{ph} \rangle$ was determined through a comparison of our optical elements and magnetic-field direction with those employed in a high-resolution resonance experiment on Rb^{85} vapor optically pumped by D_1-resonance light.[29–31]

D. Ion-Counting-Rate Asymmetry and Background Corrections

The ion-counting rates C^+ and C^- used for calculating the asymmetry δ according to Eq. (2.12) contained corrections for background effects and variations in light and atomic-beam intensities. Since data were always taken in the sequence C^+, C^-, C^-,

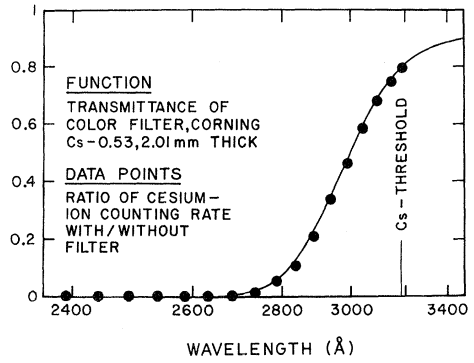

FIG. 4. Measurements demonstrating that the stray light from the monochromator did not contribute to cesium photoionization. The ratio of ion-counting rates with and without the color filter in the light beam agrees very well with the calibration of the filter transmittance furnished by Corning Glass Works.

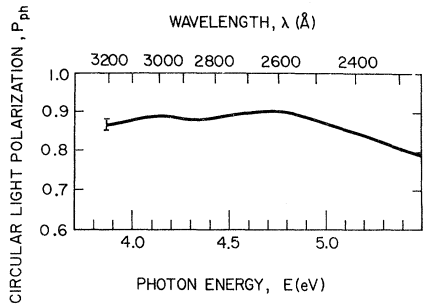

FIG. 5. Circular polarization of the photon beam as a function of the photon energy. Four different combinations of polarizer and quarter-wave plate settings were used in the experiment, which ideally should have yielded the same value for $|P_{ph}|$. In reality, slight deviations in magnitude were found as indicated by the error bar.

C^+ with the wavelength held constant, any linear variations in the product of the light and atomic-beam intensities were automatically taken into account. Small nonlinear variations were corrected with the aid of the intensity chart recordings. In the few cases where the variations were extremely nonlinear the entire data set was rejected.

Three different background counting rates were measured separately with atomic beam on, light beam off; light beam on, atomic beam off; and light beam off, atomic beam off. These corresponded to $R_{at} + R_0$, $R_{ph} + R_0$, and R_0, where R_0 is the residual counting rate with both beams off, R_{at} is the background counting rates produced by the atoms alone, and R_{ph} is the background counting rate produced by the light alone. The sum $R_{at} + R_{ph} + R_0$ was subtracted from the raw counting rates. Typical values of the background counting rates[32] were $R_{at} \approx 7$ min^{-1}, $R_{ph} \approx 5$ min^{-1}, and $R_0 \approx 3$ min^{-1}. The background correction to the counting rate varied substantially over the wavelength range covered for each alkali metal. The average correction was 10% for K, 8% for Rb, and 3% for Cs. In the worst case, the correction was 52% for K, 31% for Rb, and 11% for Cs.

An additional background effect resulted from molecular contamination of the atomic beam. Since the molecular photoionization cross sections are several orders of magnitude larger than the atomic cross sections at certain wavelengths, even a minute contamination can lead to a substantial reduction of the ion-counting-rate asymmetry δ at these wavelengths. This reduction is demonstrated in Fig. 6, which shows early data for δ/P_{ph} obtained with a cesium beam from a conventional oven and with no central beam stop installed. The photon energy range in which the data points deviate from the solid line in Fig. 6 coincides with the region in which pronounced peaks in the molecular photoionization cross section have been observed.[33] In order to eliminate this molecular effect, a two-chamber oven was designed. This measurement was not sufficient for work with potassium; consequently, a central beam stop was introduced. The data for all three alkali-metal atoms presented in Sec. IV were obtained with the central beam stop in place.

One type of background has not yet been considered; viz., ionization of alkali-metal atoms by impact of wall photoelectrons. This background appears only with both atom and photon beam "on" and therefore is not contained in R_0, R_{at}, or R_{ph}. Only photoelectrons originating at the surface of the electrode above the mouth of the Channeltron (cf. Fig. 3) which was kept at about −1 kV could have traversed the atomic beam. Great care was taken to reduce scattered light in the ionization region. The probability for an incident photon to backscatter to the electrode and to eject a photoelectron is quite small. On the other hand, the probability need be only 10^{-5} for this type of background to become serious. The cross section for alkali-metal ionization by impact of 1–2-kV electrons is probably on the order of 10^{-16} cm^2, as

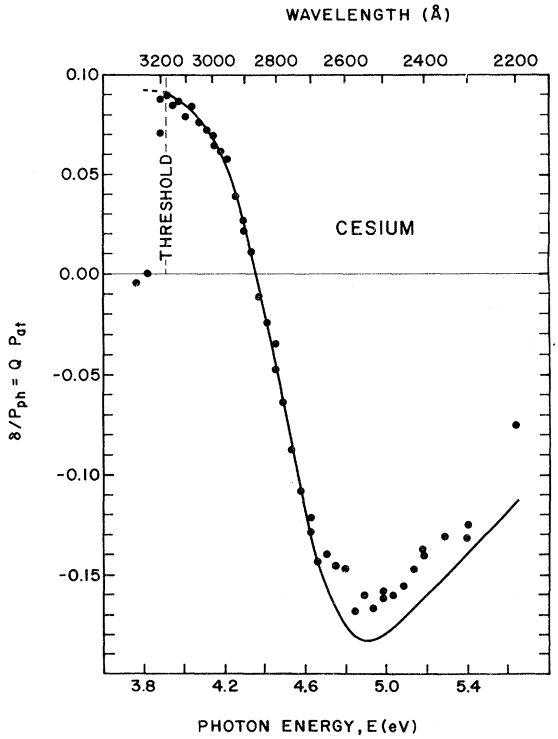

FIG. 6. Early data on δ/P_{ph} for cesium obtained before the central beam stop had been inserted at the entrance of the six-pole magnet. The solid line is a fit based upon a linear function for $x(E)$. Note the deviation of the data points from the solid line, particularly at higher photon energies. This is interpreted as an effect of photoionization of Cs_2 molecules.

judged from an extrapolation of the data of McFarland and Kinney.[34,35] By comparison, the photoionization cross section at the rubidium minimum is only 10^{-20} cm^2. Therefore this kind of background cannot be ruled out. If present, it would be most apparent near the cross-section minimum of Rb, since it is known that the photoelectron yield increases rapidly with increasing photon energy[36] and the Rb minimum lies at a higher photon energy than the K or Cs minimum.

E. Data-Evaluation Procedure

For the data evaluation a computer program was used to perform a multiparameter regression analysis.[37] Five parameters, c_1, c_2, c_3, E_0, and P_{at}, were iteratively adjusted in the function $Q(E)P_{at}$, where

$$Q = (2x-1)/(x^2+2) \tag{3.4}$$

and

$$x(E) = -c_1(E-E_0) + c_2(E-E_0)^2 + c_3(E-E_0)^3, \tag{3.5}$$

in order to obtain a best fit to the data points $\delta(E_i)/P_{ph}(E_i)$. The data points were weighted in accordance with the experimental errors in the measurement of δ/P_{ph}. The ratio (rms data)/(rms residuals) and the Durbin-Watson statistics for ordered residuals[38,39] were used as indicators of the goodness of fit. The fits obtained with the third-degree polynomial, given by Eq. (3.5) were significantly superior to fits obtained with first- and second-degree polynomials. Use of a higher-degree polynomial did not seem to be warranted (cf. Sec. V).

The computer program contained a point-by-point correction to $(\delta/P_{ph})_i$, thereby accounting for the averaging of the measured effect produced by the finite spectral width $\Delta\lambda$ of the light. Since the spectral distribution of the light source did not vary by more than 5% over the interval $(E_i - \Delta E/2, E_i + \Delta E/2)$, where $\Delta E = (dE/d\lambda)\,\Delta\lambda$, the approximation can be made that the spectral distribution is constant over this interval. The effect of the finite spectral width can then be taken into account in the following manner:

$$\delta(x_i, \Delta x) = \frac{\int_{x_i-\Delta x/2}^{x_i+\Delta x/2} (2x-1)\,dx}{\int_{x_i-\Delta x/2}^{x_i+\Delta x/2} (x^2+2)\,dx} = \frac{(2x_i-1)/(x_i^2+2)}{1+\eta_i(x_i, \Delta x)}, \tag{3.6}$$

where

$$\eta_i(x_i, \Delta x) = (\tfrac{1}{2}\Delta x)^2/3(x_i^2+2) \tag{3.7}$$

and

TABLE I. Results of data analysis.

Parameter \ Atom	Potassium	Rubidium	Cesium
c_1 (eV^{-1})	32.8 ± 3.2	9.26 ± 0.97	2.99 ± 0.13
c_2 (eV^{-2})	34 ± 16	−3.7 ± 4.0	−0.34 ± 0.32
c_3 (eV^{-3})	−76 ± 44	−5.4 ± 4.9	0.37 ± 0.53
E_0 (eV)	4.556 ± 0.005	4.955 ± 0.022	4.534 ± 0.011
P_{at}	0.254 ± 0.014	0.203 ± 0.007	0.142 ± 0.002

$$\Delta x = [dx(E)/dE]_{E=E_i}\,\Delta E\,. \tag{3.8}$$

In no case did the correction η_i exceed 0.03. The smallness of the correction indicates that the rectangular transmittance function of the monochromator, implicit in Eq. (3.6), is a sufficiently accurate representation.

IV. RESULTS

The five parameters determined by the computer fit are presented in Table I. Errors refer to 1 standard deviation. Since the errors are correlated, we have displayed the complete error matrices[40] in Table II. In Fig. 7 we have given a graphical presentation of our measurements. The data points correspond to $Q_i = a(\delta/P_{ph})_i$, where $a = (1+\eta_i)/P_{at}$. The vertical error bars, calculated from $\Delta Q_i = a\,\Delta(\delta/P_{ph})_i$, represent 1 standard deviation, while the horizontal error bars correspond to the error in the monochromator dial setting, estimated to be ±5 Å. (As explained in Sec. III E, the finite spectral width $\Delta\lambda$ is taken into account by the correction term η_i.) The curves $Q(E)$ in Fig. 7 were calculated from Eqs. (2.13) and (3.5) using the parameters given in Table I.

The main goal of our experiment was the determination of the perturbation parameter $x(E)$ over a wide energy range. In Fig. 8 are shown the functions $x(E)$ for the three alkali-metal atoms as determined from Eq. (3.5) and Table I. The error band was calculated with the aid of the error matrices given in Table II. A measure of the strength of the spin-orbit interaction is given by the energy separation of the maximum and minimum of $Q(E)$ (cf. Fig. 7) which corresponds to the zero points of R_1 and R_3, respectively. An equivalent measure is given by $(dE/dx)_0 = -1/c_1$, the reciprocal of the slope of $x(E)$ at $E = E_0$ (cf. Fig. 8 and Table I). As can be seen, the strength increases from potassium to rubidium by approximately a factor of 3.5 and from rubidium to cesium by approximately a factor of 3.

Although the quadratic and cubic coefficients c_2 and c_3 for rubidium and cesium do not have deviations from zero which are statistically significant, it should be noted that there is no theoretical reason whatever why $x(E)$ should be linear. On the contrary, from the known values of the doublet

TABLE II. Error matrices.

Parameter	c_1	c_2	c_3	E_0	P_{at}
			Potassium		
c_1	0.104 E+ 02				
c_2	0.281 E+ 02	0.255 E+ 03			
c_3	0.168 E+ 02	−0.321 E+ 03	0.196 E+ 04		
E_0	−0.126 E−01	−0.622 E−01	0.483 E−01	0.230 E−04	
P_{at}	0.345 E−01	0.172 E 00	−0.222 E 00	−0.553 E−04	0.199 E−03
			Rubidium		
c_1	0.935 E 00				
c_2	−0.142 E+ 01	0.158 E+ 02			
c_3	−0.283 E 00	0.180 E+ 02	0.242 E+ 02		
E_0	0.401 E−02	−0.670 E−01	−0.727 E−01	0.465 E−03	
P_{at}	0.435 E−02	0.110 E−02	0.580 E−02	−0.821 E−05	0.443 E−04
			Cesium		
c_1	0.170 E−01				
c_2	−0.523 E−02	0.103 E 00			
c_3	0.351 E−01	0.924 E−01	0.279 E 00		
E_0	−0.842 E−03	−0.177 E−02	−0.289 E−02	0.128 E−03	
P_{at}	0.284 E−04	−0.247 E−03	0.320 E−03	0.600 E−05	0.349 E−05

line-strength ratios of the discrete P states at low energies and the fact that both $R_3(E)$ and $R_1(E)$ must approach zero at high energies (a consequence of the f sum rule[5]), it follows that x must be a nonlinear function of E. This nonlinearity is demonstrated by the results for potassium, where the domain of E covered in the experiment corresponded to the largest range of x.

As explained above, five independent parameters were determined from a computer fit to the data points. Although the statistical indicators give a high confidence in the results obtained, an additional confidence check is provided by a comparison

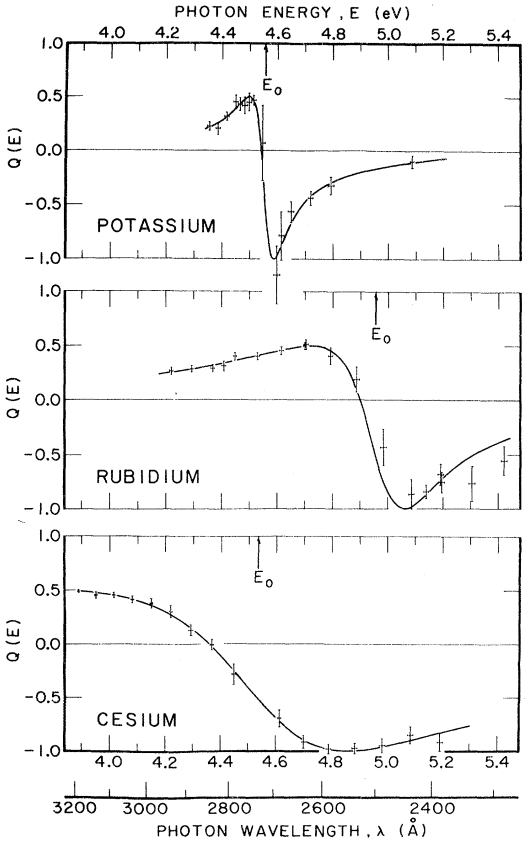

FIG. 7. Data on $Q(E)$ for potassium, rubidium, and cesium. The solid lines represent the best fit based upon a cubic function for $x(E)$.

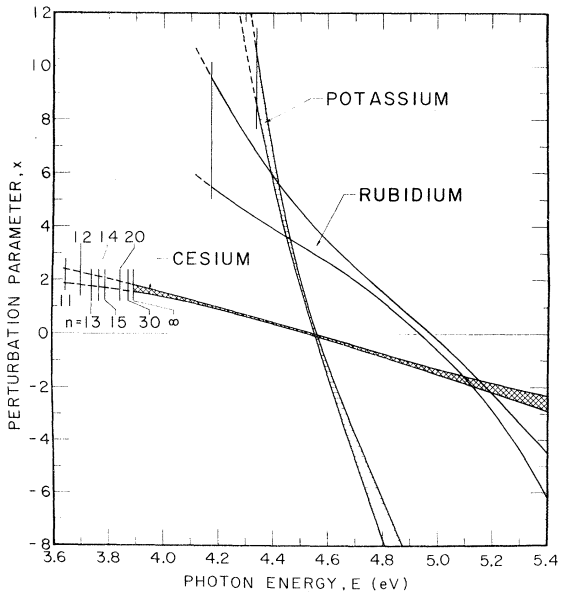

FIG. 8. Perturbation parameter $x(E)$ obtained from our measurements of $Q(E)$. The band corresponds to 1 standard deviation. Below the threshold of cesium, the energies of some of the discrete P states are indicated by vertical lines.

of the experimental value of P_{at} to an independently determined value based upon state-selection theory. The electronic polarization P_{at} of atoms state selected in a six-pole magnet can be calculated rigorously,[26] provided that the magnetic six-pole field is large compared to $\Delta W/\mu_B$, where ΔW is the hfs energy splitting and μ_B is the Bohr magneton. Beyond the six-pole magnet P_{at} is a function of the magnetic field B in the ionization region. In the limit $B \to 0$, P_{at} is given by

$$P_{at} = 1/(2I+1) . \tag{4.1}$$

Since the low-field region of the six-pole magnet was blocked by the central beam stop, the six-pole field was larger than 2000 G everywhere. From the values of $\Delta W/\mu_B$ listed in Table III it follows that Eq. (4.1) gives an exact value for P_{at} for potassium, a good approximation for rubidium, and only a lower limit for cesium. The agreement between the experimental and calculated values, shown in Table III, is excellent in the case of potassium. The deviations in the case of rubidium and cesium are exactly as expected.[41]

V. CONCLUSIONS

A. Comparison with Other Data on $x(E)$

Weisheit and Dalgarno[42,43] have recently extended their theoretical work on core-polarization effects in $n_0S \to nP$ transitions of potassium to include the effects of the spin-orbit perturbation. They employed the value $E_0 = 4.556$ eV given in Table I to set the value of the core radius at $r_c = 4.220a_0$. They then calculated $x(E)$ between threshold and 4.8 eV and obtained quantitative agreement with the potassium curve in Fig. 8. Similar calculations for rubidium and cesium, which have very recently been carried out, also show good agreement with the curves in Fig. 8.[44]

Experimental values of $x(E)$ can be inferred from measurements of $\sigma(E)$, $P(E)$, and $\rho(nP)$, among others. However, to date there exist no data which are sufficiently accurate to provide a quantitative check of our results for $x(E)$. Consequently, in Secs. V B–V D we will use our $x(E)$ to obtain information about $\sigma(E)$ and $P(E)$ for a comparison with other data available. In addition, we will extrapolate our $x(E)$ function into the discrete spectrum for a comparison with the $\rho(nP)$ data available for cesium.

TABLE III. Calculated and measured atomic polarization.

	K^{39}	K^{41}	Rb^{85}	Rb^{87}	Cs^{133}
Abundance (%)	93.1	6.9	72.15	27.85	100
Nuclear spin	$\frac{3}{2}$	$\frac{3}{2}$	$\frac{5}{2}$	$\frac{3}{2}$	$\frac{7}{2}$
hfs energy splitting $\Delta W/\mu_B$ (G)	330	82	2169	4883	6568
P_{at} obtained from calculation:					
Single isotope	0.259	0.267	0.168	0.251	0.125
Isotope mixture	0.260		0.191		0.125
Interpretation	Exact value		Approximation		Lower limit
P_{at} obtained from data analysis[a]	0.254 ± 0.014		0.203 ± 0.007		0.142 ± 0.002

[a]Error refers to 1 standard deviation.

B. Photoionization Cross Section

As shown by Eq. (2.2) knowledge of $x(E)$ can be used to evaluate $\sigma(E)$, provided some assumptions are made about $\Delta R(E)$. The ratio of the minimum to the threshold cross section σ_{min}/σ_{th} is of particular interest, since σ_{min} was predicted by Seaton[17] and σ_{th} is well known from direct measurements as well as from extrapolation of the oscillator-strength density. From Eq. (2.2) this ratio is given by

$$\sigma_{min}/\sigma_{th} = [\Delta R(E_0)/\Delta R(E_{th})]^2 (E_0/E_{th})/(1+\tfrac{1}{2}x_{th}^2) , \tag{5.1}$$

where $E_{min} \approx E_0$. From Fermi's treatment of first-order spin-orbit perturbation theory[18] for the discrete spectrum modified for the continuum transitions[2,17] we obtain

$$\Delta R(E) = \Delta\tau^{1/2}\left(\sum_{n'=n_0}^{\infty} \frac{[\Delta E(n'P)]^{1/2} R^0(n'P)}{E - E(n'P)} + \Delta\tau^{1/2}\, \mathcal{P} \int_{E_{th}}^{\infty} \frac{R^0(E')}{E-E'}\, dE' \right) , \tag{5.2}$$

where $\Delta\tau$ is the quantum-defect lag for the principal series (which to a very good approximation is independent of E), $\Delta E(n'P)$ is the fine-structure energy splitting of the $n'P$ doublet, $E(n'P)$ is the photon energy corresponding to the unperturbed $|n'P^0\rangle$ state, and $R^0(n'P)$ and $R^0(E')$ are the unperturbed radial matrix elements for transitions to the discrete and continuum P state, respectively. The symbol $\mathcal{P}$ indicates a Cauchy principal-value integral. Note that $R^0(n'P)$ and $R^0(E')$ are dimensionally different because the bound-state wave functions are normalized to unity, whereas continuum-state wave functions are normalized per unit energy interval.

From measurements of oscillator strengths and fine-structure energy intervals of discrete P states together with assumptions about the behavior of $P^0(E')$ in the continuum, $\Delta R(E)$ can be estimated according to Eq. (5.2). The function $R^0(E')$ should be consistent with experimental values of σ_{th} and x_{th}. Furthermore, $R^0(E')$ must pass through zero at $E' = E_0$, and it must approach zero at very high energies because according to the f sum rule the continuum oscillator strength must remain finite. A maximum in the cross section which must thus occur between E_0 and $E = \infty$ has not yet been observed. Given this uncertainty in the photoioniza-

TABLE IV. Alkali-metal photoionization cross sections.

Alkali metal	Authors	Ref.	Threshold value σ_{th} (Mb)	Minimum value σ_{min} (Mb)	Ratio σ_{min}/σ_{th}
Potassium	Ditchburn, Tunstead, Yates[a]	45	0.012	0.008	0.67
	Marr and Creek	46	0.007 ± 0.002	0.004 ± 0.002	0.57
	Hudson and Carter[b]	47	0.010 ± 0.002	0.002 ± 0.002	0.2
	Seaton[c]	17	[0.010]	0.0003	0.03
	Weisheit and Dalgarno[d]	43	0.006	0.00022	0.037
	This work[e]		...	...	0.02
Rubidium	Marr and Creek	46	0.100 ± 0.005	0.008 ± 0.003	0.08
	Seaton[c]	17	[0.100]	0.004	0.04
	This work[e]		...	...	0.03
Cesium	Mohler and Boeckner[a]	48	0.20	0.035	0.18
	Braddick and Ditchburn[a]	49	0.20	0.075	0.38
	Marr and Creek	46	0.20 ± 0.01	0.06 ± 0.01	0.3
	Seaton[c]	17	[0.20]	0.03	0.15
	This work[e]		...	...	0.3

[a]Data adjusted by Marr and Creek utilizing better vapor-pressure data.
[b]Note that the data are consistent with a zero-minimum cross section.
[c]Seaton gives only minimum values. The threshold values in brackets were used to calculate the cross-section ratio.
[d]These computations are based upon our measured value of E_0.
[e]Based upon Eqs. (5.1) and (5.4) and the measured threshold value of $x(E)$.

tion cross section, the function

$$R^0(E') = a(E' - E_0)e^{-b(E'-E_0)} \tag{5.3}$$

with reasonable values for the coefficients a and b, provides an acceptable model for calculation of the principal-value integral in Eq. (5.2). Evaluation of this integral leads to the tabulated exponential-integral function Ei(y) with $y = b(E - E^*)$, where E^* is the lower limit of integration. It is convenient to extend the summation only over the lowest-lying P states and to account for the higher-lying P states by extrapolating $R^0(E')$ below threshold with a correspondingly lowered integration limit $E^* < E_{th}$.

In the case of cesium for example, we found by numerical evaluation that at $E = E_{th}$ as well as at $E = E_0$ more than 70% of $\Delta R(E)$ is given by the first term of the summation in Eq. (5.2). This contribution to $\Delta R(E)$ has an energy dependence proportional to $[E - E(n_0P)]^{-1}$, where n_0P denotes the lowest P state. The energy dependence of the total ΔR can then be approximated by that of the n_0P term. We therefore used the approximation

$$\Delta R(E_0)/\Delta R(E_{th}) \approx [E_{th} - E(n_0P)]/[E_0 - E(n_0P)] \tag{5.4}$$

in conjunction with Eq. (5.1) for determining the cross-section ratio σ_{min}/σ_{th} for all three alkali metals. These results are compared with other data in Table IV.

For rubidium and cesium our values are consistent with all other data. For potassium our value lies below the experimental result of Ditchburn *et al.*[45] and that of Marr and Creek.[46] However, our value is consistent with the measurement of Hudson and Carter[47] and agrees with the theoretical calculation of Seaton[17] and that of Weisheit and Dalgarno.[43]

C. Photoelectron Polarization

Polarized electron sources are of great current interest in atomic as well as high-energy physics.[50-52] Our $x(E)$ values provide information about the relevant polarization parameter $P(E)$ [cf. Eq. (2.10)] which determines the maximum electron polarization obtainable in a Fano-type source based on photoionization of unpolarized cesium atoms by circularly polarized light. Therefore we computed $P(E)$ from our data. As the cesium parameters listed in Table I show, the coefficients c_2 and c_3 are close to zero and c_1 is very close to 3. Thus a simpler and still quite accurate description of our cesium result can be given in the form of

$$x(E)_{Cs} = -3\ \text{eV}^{-1}\ (E - 4.53\ \text{eV}), \tag{5.5}$$

which, in fact, is the one deduced from our first published results.[9] The solid line in Fig. 9 gives $P(E)$ based on Eq. (5.5). The band is the result of

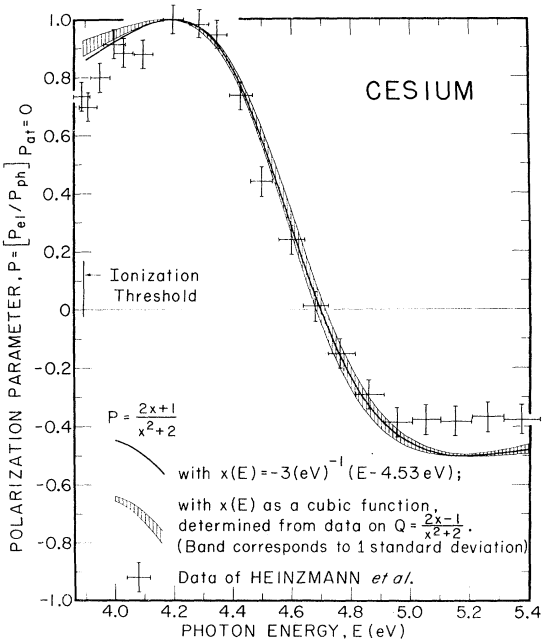

FIG. 9. Polarization parameter $P(E)$ for cesium.

the more elaborate calculation, using the best cubic function for $x(E)$ and the error matrix of Table II.

An experiment for measuring the polarization parameter P of cesium was performed by Heinzmann, Kessler, and Lorenz.[20,53] Their results are given by the data points in Fig. 9. In view of the fact that a P measurement is much more difficult than a Q measurement (cf. Sec. III A), the over-all agreement is very good, particularly in the vicinity of the zero transition of $P(E)$. Deviations exist, however, near threshold and at high photon energies. Heinzmann *et al.* in their detailed report[20] note a deviation in the zero transition of $P(E)$ between our 1969 results [Eq. (5.5) and solid line in Fig. 9] and their data. As Fig. 9 shows, this deviation does not exist.

D. Doublet Line-Strength Anomaly in Cesium

Extrapolation of $x(E)$ below threshold is of particular interest in the case of cesium because it has the largest spin-orbit perturbation. Therefore the line-strength ratio $\rho(nP)$ shows the greatest deviation from the ratio of the statistical weights, $g_{3/2}/g_{1/2} = 2$. In addition, the extrapolation of our data indicates that the energy at which $R_1 = 0$ (and $x = 2$) lies in the discrete spectrum. This energy corresponds to $\rho = +\infty$ [cf. Eq. (1.3)]. We therefore searched the literature for evidence that such a great anomaly had ever been observed.

In the older literature, the quantity referred to is the doublet-intensity (or oscillator-strength) ratio

$$r(nP) = \rho(nP)\, E(nP_{3/2})/E(nP_{1/2}) \simeq \rho(nP)\ . \tag{5.6}$$

In order to convert $\rho(nP)$ into a value of x, we rewrote Eq. (1.3) in the form

$$x(nP) = \frac{2[\rho(nP)/2]^{1/2} \pm 1}{[\rho(nP)/2]^{1/2} \mp 1}\ , \tag{5.7}$$

in which the upper signs apply to region $x > 2$, i.e., the low-energy side of the $\rho = \infty$ pole, while the lower signs apply to the region $x < 2$, i.e., the side between the pole and the ionization threshold. We have used the discrete energy values $E(nP)$ based on the spectroscopic work of Kratz.[54,55]

With increasing quantum number n, the cesium doublets get weaker and narrower very rapidly, making measurements of $r(nP)$ very difficult. Only a few investigators studied the oscillator-strength ratios of the higher nP states. Their results, together with two theoretical computations and the extrapolation of our continuum results, are presented in Fig. 10. The first investigator who extended the measurements beyond $n = 8$ was Sambursky (1928).[56] He found an increase of $r(nP)$ up to $n = 10$, followed by a marked decrease of r from $n = 10$ to $n = 13$. He presented a plot of $r(E)$ which clearly indicates a discontinuity between $n = 10$ and $n = 11$. Consequently, we used the upper signs of Eq. (4.7) for calculating the x values

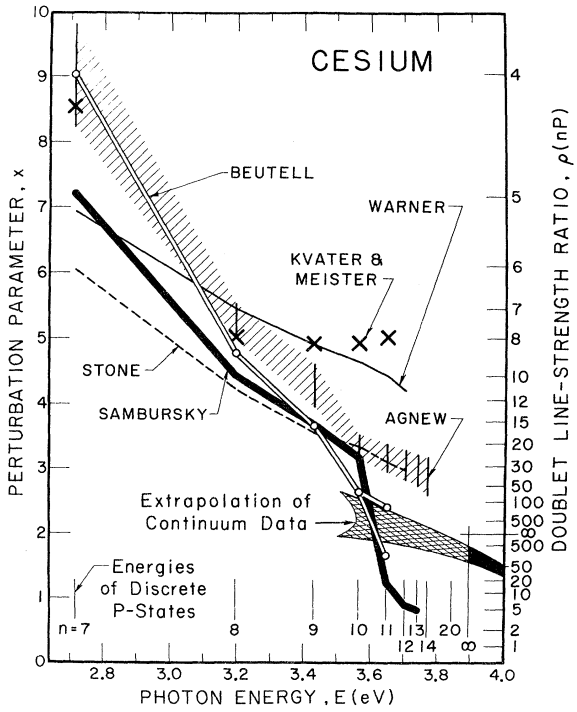

FIG. 10. Data on the perturbation parameter $x(E)$ for the discrete spectrum of cesium.

TABLE V. Experimental values for the doublet-intensity ratios, for the cesium P states with $n=7$ and 8.

Year	Author	Ref.	Method	$r(7)$	$r(8)$
1914	Füchtbauer and Hofmann	63	Absorption	~3	3–4
1921	Bartels	64	Absorption	•••	5.00, 5.23
1921	Roshdestvenski	65	Dispersion	4.07	7.4
1924	Rasetti	66	Magneto-optics	3.85 ± 0.09	•••
1926	Kohn and Jakob	67	Emission	~4	•••
1926	Füchtbauer and Maier	68	Absorption	•••	5.6
1927	Filippov	69	Emission	3–4	•••
1927	Hagenow and Hughes	70	Emission	3.58	•••
1928	Sambursky	56	Emission	5	10
1928	Jakob	71	Emission	4.0	•••
1929	Füchtbauer and Wolff	72	Emission	3.3	4.6
1929	Bleeker	73	Emission	5.5	•••
1930	Minkowski and Mühlenbruch	74	Magneto-optics	4.27 ± 0.12	•••
1930	Schütz	75	Absorption	3	•••
1933	Kohn and Hübner	76	Emission	•••	8.0 ± 0.3
1939	Beutell	58	Emission	4.1	8.7
1952	Kvater and Meister	59	Dispersion	4.285	8.0
1966	Agnew	61	Absorption	4.15 ± 0.28	7.63 ± 0.76

corresponding to Sambursky's results for $n \leq 10$ and the lower signs, for $n \geq 11$. To date, no one has been able to verify this decrease of r for the higher nP states; on the contrary, subsequent investigators have contradicted Sambursky's work. This started in 1929, when Waibel[57] reported $r(10) = 5.3$ and $r(11) = 10.0$ (not included in Fig. 10). In 1939 Beutell[58] measured r values which are the largest ever observed: $r(10) = 50–80$ and $r(11) = 110–170$. Since it is not clear, to which side of the pole this latter value belongs, we plotted two branches for Beutell in Fig. 10. In 1949 Kratz[54] published his measurements on the cesium lines, and for the doublets resolved up to $n = 21$ he stated, "... an inspection of the cesium plates shows not the decrease observed by Sambursky, but rather an increase in the ratios, perhaps to an asymptotic value, with increasing principal quantum number." Kvater and Meister (1952)[59] obtained r values no larger than 8.1 for $n = 8$ through $n = 11$. What is notable is the vigor with which Kvater and Meister criticize Sambursky as well as Beutell. The calculations of Stone (1962)[60] are based on one-electron wave functions in a central potential, tailored to give good reproduction for the discrete energy levels. Stone calculated the oscillator strengths with the inclusion of a spin-orbit term which led to the x values plotted as the dashed line in Fig. 10. The most recent experimental data are those of Agnew (1966),[61] which are in good agreement with Stone's results in the range of higher n. In a calculation which takes into account not only the differences in wave functions due to spin-orbit interaction, but also the configuration mixing caused by that interaction, Warner (1968)[62] obtained results corresponding to the thin solid line in Fig. 10. In summary, all the more recent work, experimental as well as theoretical, yields x values which lie considerably above the extrapolation of our $x(E)$ data.

Our data support the assumption that the results of the early work of Sambursky and Beutell have more validity than later critics were willing to concede. We do not know the reasons for the discrepancies exhibited in Fig. 10. Doublet oscillator-strength ratios are difficult to measure. Even for the lower states $n = 7$ and 8, for which oscillator strengths and energy splittings are large, the experimental results of different authors show considerable variation, as exhibited in Table V. The papers referred to give detailed accounts of the technical problems with which each one of those experiments was beset. Nevertheless, modern spectroscopy should yield a definite answer to the existing discrepancies. Work with that aim is currently being pursued.[77]

ACKNOWLEDGMENTS

We gratefully acknowledge the encouragement and support given by Professor V. W. Hughes. We also wish to thank D. Constantino for his technical assistance and Miss Laurie LeQuire for her help with the preparation of the manuscript.

†Work supported in part by the U.S. Office of Naval Research, Contract No. N00014-67-A-0097-0015.

[1]U. Fano, Comments At. Mol. Phys. 2, 30 (1970).

[2]U. Fano, Phys. Rev. 178, 131 (1969).

[3]W. Hanus, Bull. Acad. Polon. Sci., Ser. Sci. Math. Astron. Phys. 13, 73 (1965).

[4]G. zu Putlitz, Comments At. Mol. Phys. 1, 51 (1969).
[5]G. V. Marr and D. M. Creek, Proc. Roy. Soc. (London) A304, 245 (1968).
[6]F. S. Ham, in *Solid State Physics*, edited by F. Seitz and D. Turnbull (Academic, New York, 1955), Vol. I, p. 127; T. S. Kuhn, Phys. Rev. 79, 515 (1950).
[7]M. J. Seaton, Comments At. Mol. Phys. 2, 37 (1970).
[8]M. S. Lubell and W. Raith, in *Proceedings of the Sixth International Conference on the Physics of Electronic and Atomic Collisions, Cambridge, Massachusetts*, 1969 (MIT Press, Cambridge, Mass., 1969), p. 771.
[9]M. S. Lubell and W. Raith, Phys. Rev. Letters 23, 211 (1969).
[10]G. Baum, M. S. Lubell, and W. Raith, Bull. Am. Phys. Soc. 14, 950 (1969).
[11]G. Baum, M. S. Lubell, and W. Raith, Bull. Am. Phys. Soc. 15, 559 (1970).
[12]G. Baum, M. S. Lubell, and W. Raith, Abstracts of the Second International Conference on Atomic Physics, Oxford, England, 1970, p. 22 (unpublished).
[13]G. Baum, M. S. Lubell, and W. Raith, Phys. Rev. Letters 25, 267 (1970).
[14]W. Raith, Bull. Am. Phys. Soc. 16, 487 (1971).
[15]U. Fano and J. W. Cooper, Rev. Mod. Phys. 40, 441 (1968).
[16]J. W. Cooper, Phys. Rev. 128, 681 (1962).
[17]M. J. Seaton, Proc. Roy. Soc. (London) A208, 408 (1951).
[18]E. Fermi, Z. Physik 59, 680 (1930).
[19]G. V. Marr and D. M. Creek, Proc. Roy. Soc. (London) A304, 233 (1968).
[20]U. Heinzmann, J. Kessler, and J. Lorenz, Z. Physik 240, 42 (1970).
[21]J. Kessler, Physik. Blätter 27, 161 (1971).
[22]U. Fano, Phys. Rev. 184, 250 (1969).
[23]These figures are based on the following estimates: photons, $\mathcal{P} \sim 0.9$, $\eta \sim 0.2$ (in near uv); atoms, $\mathcal{P} \sim 0.15$, $\eta \sim 0.2$ (for low-field polarization produced by state selection in a six-pole magnet which has favorable focusing properties); electrons, $\mathcal{P} \sim 0.25$, $\eta \sim 10^{-5}$ (for Mott scattering from a gold foil, the most commonly used technique).
[24]B. Brehm, Z. Physik 242, 195 (1971).
[25]G. Baum, M. S. Lubell, and W. Raith, Bull. Am. Phys. Soc. 16, 586 (1971).
[26]V. W. Hughes, R. L. Long, Jr., M. S. Lubell, M. Posner, and W. Raith, Phys. Rev. A 5, 195 (1972).
[27]All measurements were made with $\Delta\lambda = 16$ Å, except, three data points for rubidium (at $\lambda = 2387$, 2412, and 2637 Å), which were obtained with $\Delta\lambda = 32$ Å.
[28]M. Born and E. Wolf, *Principles of Optics*, 2nd ed. (MacMillan, New York, 1964), p. 31.
[29]E. S. Ensberg, Phys. Rev. 153, 36 (1967).
[30]G. S. Hayne, E. S. Ensberg, and H. G. Robinson, Phys. Rev. 171, 20 (1968).
[31]This determination was carried out with the cooperation of Dr. E. S. Ensberg of Yale University.
[32]In footnote 10 of Ref. 9 it was reported that "a rather high background counting rate" was observed when the atomic beam was on and the light beam off. All the data contained in the present paper were obtained after this background, R_{at}, had been reduced by two orders of magnitude. The Channeltron was partially enclosed in a metal box, and the oven heater was biased positively. The effect of the heater bias indicates that the previously large value of R_{at} was somehow related to electron impact phenomena in the oven chamber. The details of these phenomena were not investigated.
[33]D. M. Creek and G. V. Marr, J. Quant. Spectry. Radiative Transfer 8, 1431 (1968).
[34]R. H. McFarland and J. D. Kinney, Phys. Rev. 137, A1058 (1965).
[35]L. J. Kieffer and G. H. Dunn, Rev. Mod. Phys. 38, 1 (1966).
[36]I. Ames and R. L. Christensen, in *Methods of Experimental Physics*, edited by L. Marton, V. W. Hughes, and H. L. Schultz (Academic, New York, 1967), Vol. 4A, p. 53.
[37]A large part of the program was provided by Dr. D. L. Mader and Dr. W. H. Wing of Yale University.
[38]J. Durbin and G. S. Watson, Biometrika 37, 409 (1950); 38, 159 (1951).
[39]H. Theil and A. L. Nagar, Am. Statist. Assoc. J. 793 (1961).
[40]J. Mathews and R. L. Walker, *Mathematical Methods of Physics* (Benjamin, New York, 1965), p. 367.
[41]With a central beam stop inserted at the six-pole magnet entrance, only atoms in Zeeman states $|m_s = +\frac{1}{2}, m_I\rangle$ can pass through the magnet. If the magnetic field in the ionization region is close to zero, the electronic polarization of the atoms in the individual states $|+\frac{1}{2}, m_I\rangle$ is given by $\langle\sigma_z(+\frac{1}{2}, m_I)\rangle = (2m_I+1)/(2I+1)$, which ranges from $\langle\sigma_z\rangle = 1$ for $m_I = +I$ to $\langle\sigma_z\rangle = -(2I-1)/(2I+1)$ for $m_I = -I$. Only if the transmittance solid angle of the six-pole magnet is independent of m_I will the $2I+1$ different Zeeman states be populated equally and only then will the average electronic polarization be given by $P_{at} = 1/(2I+1)$. If, however, the six-pole field is not large compared with $\Delta W/\mu_B$, the effective magnetic moment of the atom and therefore the transmittance solid angle will depend on m_I. The dependence is such that beyond the six-pole magnet the atomic beam will contain more atoms in states with positive m_I (for which $\langle\sigma_z\rangle > 0$) than in states with negative m_I (for which $\langle\sigma_z\rangle \leq 0$). Consequently, the average electronic polarization will be higher than $1/(2I+1)$. This explains why we obtained $P_{at}(\mathrm{Cs}) = 0.142$ as compared to 0.125, the value based strictly on the formula $P_{at} = 1/(2I+1)$ with $I = \frac{7}{2}$. This deviation will be even larger if the weak-field region of the six-pole magnet is not blocked by the beam stop. Indeed, we observed this in our early measurements. This is demonstrated by the solid line in Fig. 6 which corresponds to $P_{at}(\mathrm{Cs}) = 0.184$.
[42]J. C. Weisheit and A. Dalgarno, Chem. Phys. Letters 9, 517 (1971).
[43]J. C. Weisheit and A. Dalgarno, Phys. Rev. Letters 27, 701 (1971).
[44]J. C. Weisheit (unpublished).
[45]R. W. Ditchburn, J. Tunstead, and J. G. Yates, Proc. Roy. Soc. (London) A181, 386 (1943).
[46]G. V. Marr and D. M. Creek, Proc. Roy. Soc. (London) A304, 233 (1968).
[47]R. D. Hudson and V. L. Carter, Phys. Rev. 139, A1426 (1965).
[48]F. L. Mohler and C. Boeckner, J. Res. Natl. Bur. Std. (U.S.) 3, 303 (1929).
[49]H. J. J. Braddick and R. W. Ditchburn, Proc. Roy. Soc. (London) A143, 472 (1934).
[50]W. Raith, in *Atomic Physics*, edited by V. W. Hughes, B. Bederson, V. W. Cohen, and F. M. J. Pichanick (Plenum, New York, 1969), p. 389.

[51]B. Bederson, Phys. Today 22 (No. 11), 87 (1969).
[52]J. Bjorken and E. A. Paschos, Phys. Rev. 185, 1975 (1969).
[53]U. Heinzmann, J. Kessler, and J. Lorenz, Phys. Rev. Letters 25, 1325 (1970).
[54]H. R. Kratz, Phys. Rev. 75, 1844 (1949).
[55]C. E. Moore, in *Atomic Energy Levels*, Natl. Bur. Std. (U.S.) Circ. No. 467 (U.S. GPO, Washington, D.C., 1949), Vol. I, p. 227.
[56]S. Sambursky, Z. Physik 49, 731 (1928).
[57]F. Waibel, Z. Physik 53, 459 (1929).
[58]M. Beutell, Ann. Physik 36, 533 (1939).
[59]G. S. Kvater and T. G. Meister, Vestnik. Leningrad. Univ. 9, 137 (1952); *Optical Transition Probabilities* (National Science Foundation, Israel Program for Scientific Translations, Jerusalem, 1962), p. 191.
[60]P. M. Stone, Phys. Rev. 127, 1151 (1962).
[61]L. Agnew, Bull. Am. Phys. Soc. 11, 327 (1966).
[62]B. Warner, Monthly Notices Roy. Astron. Soc. 139, 115 (1968).
[63]C. Füchtbauer and W. Hofmann, Ann. Physik 43, 96 (1914).
[64]H. Bartels, Ann. Physik 65, 143 (1921).
[65]D. S. Roshdestvenski, Trans. Opt. Inst. Petrograd II 13, 1 (1921).
[66]F. Rasetti, Nuovo Cimento 1, 115 (1924).
[67]H. Kohn and H. Jakob, Physik. Z. 27, 819 (1926).
[68]C. Füchtbauer and H. Maier, Physik. Z. 27, 853 (1926).
[69]A. Filippov, Z. Physik 36, 477 (1926).
[70]C. F. Hagenow and A. L. Hughes, Phys. Rev. 30, 284 (1927).
[71]H. Jakob, Ann. Physik 86, 449 (1928).
[72]C. Füchtbauer and H. W. Wolff, Ann. Physik 3, 359 (1929).
[73]W. Bleeker, Z. Physik 52, 808 (1929).
[74]R. Minkowski and W. Mühlenbruch, Z. Physik 63, 198 (1930).
[75]W. Schütz, Z. Physik 64, 682 (1930).
[76]H. Kohn and H. J. Hübner, Physik. Z. 34, 278 (1933); H. J. Hübner, Ann. Physik 17, 781 (1933).
[77]H. Stroke (private communication).

PHYSICAL REVIEW A VOLUME 5, NUMBER 3 MARCH 1972

Further Calculations on Multiple-Quantum Transitions*

C. S. Chang and P. Stehle
Physics Department, University of Pittsburgh, Pittsburgh, Pennsylvania 15213
(Received 21 July 1971)

We develop a detailed theory to calculate multiple-quantum transition probabilities. It is shown that the quantum electrodynamical (QED) approach must be used in order to explain quantitatively the experimental observations of Kusch. The anomalous behavior of shifts in resonance frequency and saturation of widths of transition probabilities can be explained on the basis of a QED renormalization principle. In this paper, we work out the detailed calculations for the case of a double-quantum transition quantitatively. The agreement between QED calculation and Kusch's observation is remarkable. We conclude that the renormalization principle of QED is important even for low-frequency and finite-intensity fields.

I. INTRODUCTION

In an earlier paper[1] a quantum electrodynamic (QED) theory of induced transitions in atoms and molecules was developed and shown to be distinct from the semiclassical theory when the inducing field is not weak. In this paper the methods developed are applied in detail to the experiments of Kusch[2] resulting in excellent agreement between theory and observation. No such agreement can be obtained by applying the semiclassical theory.

Kusch used a five-level system, so that a theoretical discussion requires the use of higher orders in perturbation theory. When orders higher than the lowest nontrivial order are included, it is necessary to include renormalization effects produced by forward scattering processes just as in higher-order radiative correction calculations it is necessary to take wave-function renormalization produced by virtual-photon processes into account.[3] In Sec. II this renormalization procedure is developed, and in Sec. III it is applied to a double-quantum transition observed by Kusch, yielding both the lineshift and the linewidth as functions of inducing field strength. The results are compared with observation and with the semiclassical results obtained by Salwen.[4] In Sec. IV some comments on the method and its relation to the Majorana formula[5] are given.

II. RENORMALIZATION BY FORWARD SCATTERING

The Green's function for an electron moving in a static potential $V(\vec{r})$ and in a radiation field with one mode excited satisfies the Schwinger-Dyson equation given in I, namely,

$$G(x,x') = S_F(x,x') - i\int d^4x''d^4x''' S_F(x,x'') \times M(x'',x''')G(x''',x') , \quad (1)$$

where $S_F(x,x')$ is the propagator in the static field